

# Müntz-Szász Networks:

## Neural Architectures with Learnable Power-Law Bases

Gnankan Landry Regis N'guessan<sup>1,2,3</sup>

<sup>1</sup>Axiom Research Group

<sup>2</sup>Department of Applied Mathematics and Computational Science,  
The Nelson Mandela African Institution of Science and Technology (NM-AIST),  
Arusha, Tanzania

<sup>3</sup>African Institute for Mathematical Sciences (AIMS),  
Research and Innovation Centre (RIC), Kigali, Rwanda

[rnguessan@aimsric.org](mailto:rnguessan@aimsric.org)

### Abstract

Standard neural network architectures employ fixed activation functions (ReLU, tanh, sigmoid) that are poorly suited for approximating functions with singular or fractional power behavior, a structure that arises ubiquitously in physics, including boundary layers, fracture mechanics, and corner singularities. We introduce **Müntz-Szász Networks (MSN)**, a novel architecture that replaces fixed smooth activations with learnable fractional power bases grounded in classical approximation theory. Each MSN edge computes  $\phi(x) = \sum_k a_k |x|^{\mu_k} + \sum_k b_k \text{sign}(x) |x|^{\lambda_k}$ , where the exponents  $\{\mu_k, \lambda_k\}$  are learned alongside the coefficients. We prove that MSN inherits universal approximation from the Müntz-Szász theorem and establish novel approximation rates: for functions of the form  $|x|^\alpha$ , MSN achieves error  $\mathcal{O}(|\mu - \alpha|^2)$  with a *single* learned exponent, whereas standard multilayer perceptrons (MLPs) require  $\mathcal{O}(\epsilon^{-1/\alpha})$  neurons for comparable accuracy. On supervised regression with singular target functions, MSN achieves **5-8× lower error** than MLPs with **10× fewer parameters**. Physics-informed neural networks (PINNs) represent a particularly demanding application for singular function approximation; on PINN benchmarks including a singular ordinary differential equation (ODE) and stiff boundary-layer problems, MSN achieves **3-6× improvement** while learning interpretable exponents that match the known solution structure. Our results demonstrate that theory-guided architectural design can yield dramatic improvements for scientifically-motivated function classes.

**Keywords:** neural networks, approximation theory, physics-informed neural networks, Müntz-Szász theorem, Müntz spaces, learnable activations, singular functions, power-law bases, fractional exponents

# 1 Introduction

Neural networks have achieved remarkable success across diverse domains, yet their effectiveness depends critically on matching architectural inductive biases to problem structure. Standard architectures employ smooth activation functions ( $\tanh$ ,  $\text{sigmoid}$ ) or piecewise-linear functions (ReLU), which are universal approximators but poorly suited for functions with singular or fractional power behavior. Such functions arise ubiquitously in physics: boundary layers exhibit  $\mathcal{O}(\epsilon^{1/2})$  thickness scaling [Schlichting and Gersten, 2017], crack-tip stresses scale as  $r^{-1/2}$  in fracture mechanics [Anderson, 2005], and corner singularities in elliptic partial differential equations (PDEs) produce solutions of the form  $r^{\pi/\omega}$  where  $\omega$  is the corner angle [Grisvard, 2011].

Physics-informed neural networks (PINNs) [Raissi et al., 2019] embed physical laws directly into the learning objective, enabling mesh-free solutions to differential equations. However, PINNs inherit the approximation limitations of their underlying architectures. For a function  $f(x) = |x|^\alpha$  with  $0 < \alpha < 1$ , achieving approximation error  $\epsilon$  requires  $\mathcal{O}(\epsilon^{-1/\alpha})$  ReLU neurons [Yarotsky, 2017], an exponential cost in the singularity strength. This limitation manifests in practice as PINN failures on stiff boundary-layer problems [Krishnapriyan et al., 2021] and high errors near singularities.

We propose a fundamentally different approach: rather than approximating singular functions with smooth or piecewise-linear bases, we *learn the exponents directly*. Our architecture is grounded in the classical Müntz-Szász theorem [Müntz, 1914, Szász, 1916], which characterizes when power functions with arbitrary real exponents form a complete basis:

**Theorem 1** (Müntz-Szász, 1914). *The span of  $\{1, x^{\lambda_1}, x^{\lambda_2}, \dots\}$  with  $0 < \lambda_1 < \lambda_2 < \dots$  is dense in  $C[0, 1]$  if and only if  $\sum_{k=1}^{\infty} 1/\lambda_k = \infty$ .*

This theorem guarantees that with appropriately chosen exponents, power functions can approximate *any* continuous function, including those with fractional power structure. Our **Müntz-Szász Networks (MSN)** leverage this insight by learning the exponents  $\{\mu_k, \lambda_k\}$  alongside the coefficients, enabling the network to discover and exploit the natural power structure of the target function. MSN is a general-purpose approximation architecture for functions with power-law structure; PINNs represent a particularly demanding application where this structure commonly arises.

To address these limitations, we introduce Müntz-Szász Networks and make the following contributions:

1. **Architecture:** We introduce MSN, a neural network architecture where each edge computes a Müntz polynomial with learnable exponents. We develop a bounded parameterization ensuring numerical stability and propose a Müntz divergence regularizer connecting to classical approximation theory (Section 3).
2. **Theory:** We prove universal approximation for MSN (Theorem 3) and establish novel approximation rates showing MSN achieves  $\mathcal{O}(\delta^2)$  error for

power functions when the learned exponent is within  $\delta$  of the true exponent (Theorem 4), compared to  $\mathcal{O}(N^{-2\alpha})$  for MLPs (Section 4).

3. **Experiments:** On supervised regression with singular functions ( $\sqrt{x}$ ,  $|x - 0.5|^{0.2}$ ), MSN achieves  $5\text{-}8\times$  lower error than MLPs with  $10\times$  fewer parameters. On PINN benchmarks (singular ODE, boundary-layer boundary value problems), MSN achieves  $3\text{-}6\times$  improvement while learning interpretable exponents (Section 5).

## 2 Background

### 2.1 The Müntz-Szász Theorem

The Müntz-Szász theorem, originating in the work of Müntz [Müntz, 1914] and Szász [Szász, 1916], provides a complete characterization of when systems of monomials with non-integer exponents form a dense subset of  $C[0, 1]$ . Together with the Weierstrass approximation theorem, it stands as a cornerstone of constructive approximation theory, addressing the fundamental question of which function systems can represent arbitrary continuous functions. For comprehensive treatments, see Borwein and Erdélyi [1995] and Lorentz et al. [1996].

**Definition 1** (Müntz System). *For a sequence  $\Lambda = \{0 \leq \lambda_0 < \lambda_1 < \dots\}$ , the Müntz system is  $\mathcal{M}_\Lambda = \{x^{\lambda_k}\}_{k=0}^\infty$ .*

The divergence condition  $\sum_{k=1}^\infty 1/\lambda_k = \infty$  in Theorem 1 ensures that exponents do not grow too rapidly. For example,  $\Lambda = \{0, 1, 2, 3, \dots\}$  (polynomials) trivially satisfies the condition, as does  $\Lambda = \{0, 0.5, 1, 1.5, 2, \dots\}$ . However,  $\Lambda = \{0, 2, 4, 8, 16, \dots\}$  violates it, and indeed the span of  $\{1, x^2, x^4, x^8, \dots\}$  cannot approximate  $x$  on  $[0, 1]$ .

For symmetric intervals, we require the *full Müntz theorem*:

**Theorem 2** (Full Müntz Theorem). *Let  $0 < \lambda_1 < \lambda_2 < \dots$  with  $\sum_k 1/\lambda_k = \infty$ . Then the system*

$$\{1\} \cup \{|x|^{\lambda_k}\}_{k=1}^\infty \cup \{\text{sign}(x)|x|^{\lambda_k}\}_{k=1}^\infty$$

*is dense in  $C[-1, 1]$ .*

The constant function 1 is essential for approximating functions  $f$  with  $f(0) \neq 0$ , since  $|0|^\lambda = 0$  for all  $\lambda > 0$ . The even functions  $|x|^\lambda$  and odd functions  $\text{sign}(x)|x|^\lambda$  together decompose any continuous function on symmetric domains.

**Remark 1** (Relationship to Classical Theory). *We emphasize that MSNs do not implement the Müntz-Szász theorem in its classical form. The theorem concerns uniform density of infinite monomial systems in  $C[0, 1]$ , whereas MSNs operate with finite, learned exponent sets, empirical loss functions (typically  $L^2$ ), and compositional architectures. In this sense, the theorem serves as a guiding principle rather than a direct blueprint: it motivates the use of learnable power bases and informs the design of our regularizer, but the network itself is a*

*finite, trainable approximation. Empirical risk minimization and compositional architectures are necessary to scale beyond classical approximation settings and to integrate with modern learning pipelines.*

## 2.2 Physics-Informed Neural Networks

PINNs [Raissi et al., 2019] solve differential equations by training neural networks to satisfy physical laws. For a PDE  $\mathcal{N}[u](\mathbf{x}) = 0$  on domain  $\Omega$  with boundary conditions  $\mathcal{B}[u](\mathbf{x}) = g(\mathbf{x})$  on  $\partial\Omega$ , the PINN loss is:

$$\mathcal{L} = \frac{1}{N_c} \sum_{i=1}^{N_c} |\mathcal{N}[u_\theta](\mathbf{x}_i)|^2 + \lambda_{BC} \frac{1}{N_b} \sum_{j=1}^{N_b} |\mathcal{B}[u_\theta](\mathbf{x}_j) - g(\mathbf{x}_j)|^2, \quad (1)$$

where derivatives are computed via automatic differentiation.

PINNs face several challenges for singular solutions:

- **Spectral bias:** Networks learn low-frequency components before high-frequency ones [Rahaman et al., 2019, Wang et al., 2021b], causing slow convergence near singularities.
- **Gradient pathologies:** Imbalanced loss terms cause unstable training [Wang et al., 2021a].
- **Representation limits:** Smooth activations cannot efficiently represent fractional powers [Yarotsky, 2017].

MSN addresses the third challenge directly by learning appropriate power bases, potentially alleviating the first two as well.

## 3 Müntz-Szász Networks

We now introduce Müntz-Szász Networks (MSN), beginning with the basic building block and progressing to the full architecture.

### 3.1 Architecture

**Definition 2** (Müntz Edge). *A Müntz edge  $\phi : \mathbb{R} \rightarrow \mathbb{R}$  is defined as*

$$\phi(x; \mathbf{a}, \mathbf{b}, \boldsymbol{\mu}, \boldsymbol{\lambda}) = \sum_{k=1}^{K_e} a_k |x|^{\mu_k} + \sum_{k=1}^{K_o} b_k \text{sign}(x) |x|^{\lambda_k}, \quad (2)$$

where  $\boldsymbol{\mu} = (\mu_1, \dots, \mu_{K_e}) \in \mathbb{R}_{>0}^{K_e}$  are even exponents,  $\boldsymbol{\lambda} = (\lambda_1, \dots, \lambda_{K_o}) \in \mathbb{R}_{>0}^{K_o}$  are odd exponents, and  $\mathbf{a}, \mathbf{b}$  are learnable coefficients.

The decomposition into even ( $|x|^\mu$ ) and odd ( $\text{sign}(x)|x|^\lambda$ ) terms mirrors the parity decomposition of functions on symmetric domains and is justified by Theorem 2.

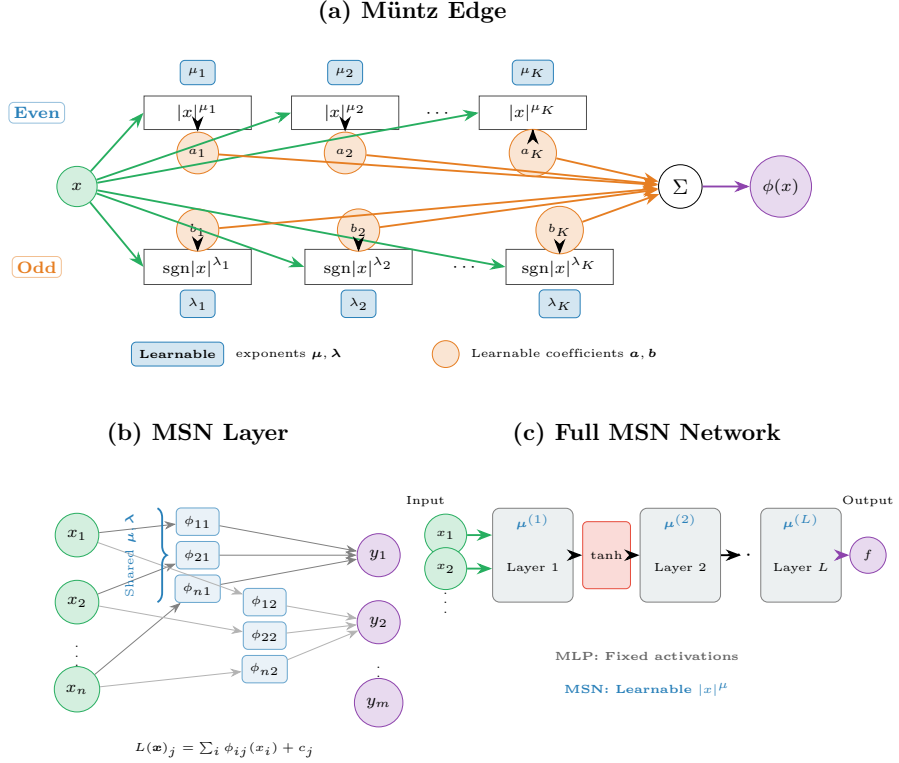


Figure 1: **Müntz-Szász Network architecture.** (a) A Müntz edge computes  $\phi(x) = \sum_k a_k |x|^{\mu_k} + \sum_k b_k \text{sgn}(x) |x|^{\lambda_k}$  with learnable exponents  $\mu, \lambda$  and coefficients  $a, b$ . (b) An MSN layer connects all input-output pairs via Müntz edges with shared exponents. (c) Full MSN stacks layers with inter-layer nonlinearities (tanh). Unlike standard networks with fixed activations, MSN learns the functional form of each edge.

**Definition 3** (MSN Layer). *An MSN layer  $L : \mathbb{R}^{d_{in}} \rightarrow \mathbb{R}^{d_{out}}$  is:*

$$L(\mathbf{x})_j = \sum_{i=1}^{d_{in}} \phi_{ij}(x_i) + c_j, \quad j = 1, \dots, d_{out}, \quad (3)$$

where each  $\phi_{ij}$  is a Müntz edge and  $c_j$  are bias terms.

**Definition 4** (Müntz-Szász Network). *A Müntz-Szász Network with  $L$  layers is:*

$$f_{MSN}(\mathbf{x}) = L_L \circ \tau \circ L_{L-1} \circ \tau \circ \dots \circ \tau \circ L_1(\mathbf{x}), \quad (4)$$

where  $\tau = \tanh$  is applied elementwise between layers.

## Müntz-Szász Network (MSN)

*Learnable Fractional Power Bases*

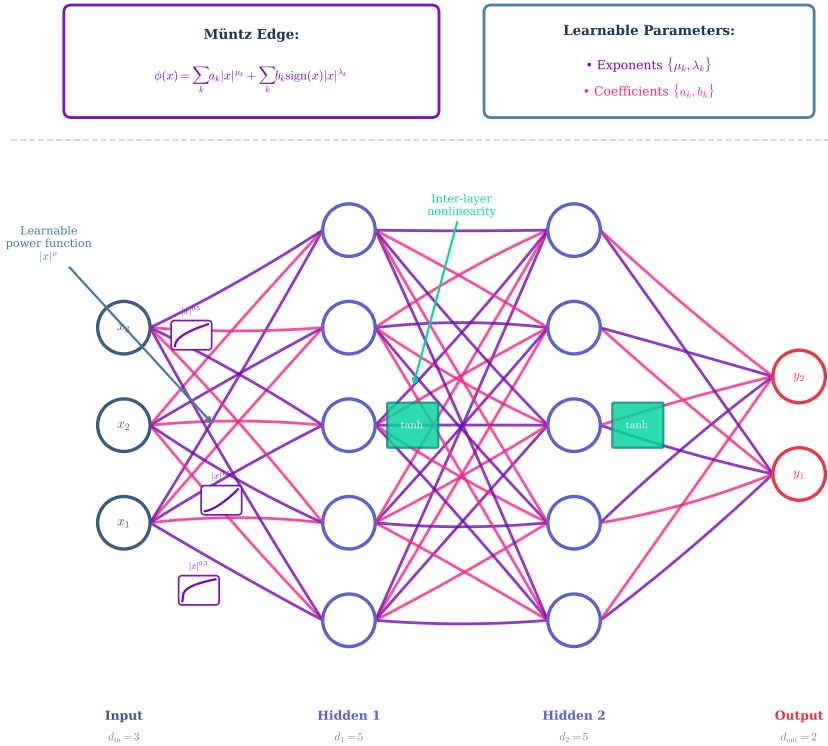


Figure 2: **Full MSN architecture with learnable power functions.** The network transforms inputs through MSN layers connected by tanh nonlinearities. Small inset plots on representative edges visualize the learned power functions (e.g.,  $|x|^{0.3}$ ,  $|x|^{0.5}$ ,  $|x|^{1.5}$ ). This architecture enables MSN to discover and exploit the natural power structure of target functions.

## MLP vs MSN: Architectural Comparison

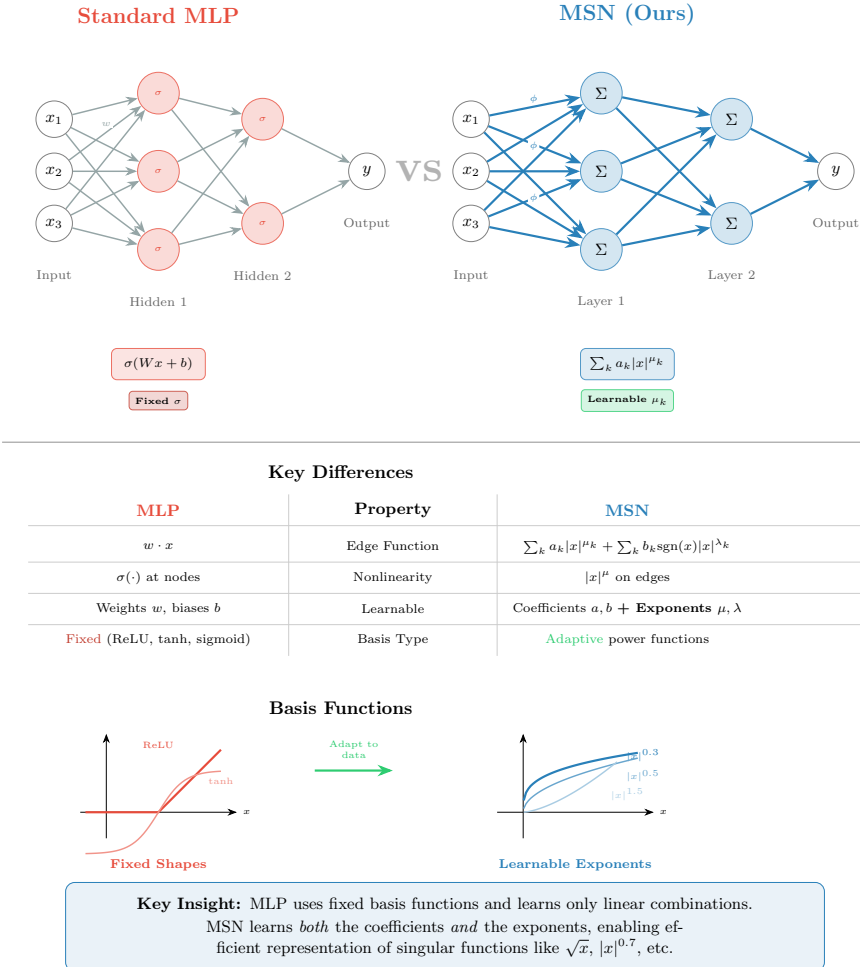


Figure 3: **Comparison of MLP and MSN architectures.** MLP uses fixed activation functions (ReLU, tanh) at nodes and learns only weights on edges. MSN uses learnable power functions  $|x|^{\mu_k}$  on edges, learning both coefficients and exponents. This enables efficient representation of singular functions.

**Exponent Sharing.** In practice, we share exponents  $(\boldsymbol{\mu}, \boldsymbol{\lambda})$  across all edges within a layer, reducing exponent parameters from  $\mathcal{O}(d_{\text{in}} \cdot d_{\text{out}} \cdot K)$  to  $\mathcal{O}(K)$  per layer while maintaining distinct coefficients  $(\mathbf{a}, \mathbf{b})$  per edge.

### 3.2 Exponent Parameterization

Directly optimizing exponents in  $\mathbb{R}_{>0}$  is numerically unstable: gradients can push exponents negative (undefined) or extremely large (overflow for  $|x| > 1$ ). We propose a *bounded parameterization* ensuring well-behaved exponents.

**Definition 5** (Bounded Exponent Map). *For raw parameters  $\mathbf{r} \in \mathbb{R}^K$ , maximum exponent  $p_{\max} > 0$ , and margin  $\varepsilon > 0$ :*

$$\mu_k = \varepsilon + (p_{\max} - 2\varepsilon) \cdot \text{sort}(\sigma(\mathbf{r}))_k, \quad (5)$$

where  $\sigma(r) = 1/(1 + e^{-r})$  is the sigmoid function.

**Proposition 1** (Properties of Bounded Parameterization). *The map  $\mathbf{r} \mapsto \boldsymbol{\mu}$  satisfies:*

1. **Strict positivity:**  $\mu_k \in (\varepsilon, p_{\max} - \varepsilon)$  for all  $k$ .
2. **Ordering:**  $\mu_1 < \mu_2 < \dots < \mu_K$  almost surely.
3. **Differentiability:** The map is differentiable almost everywhere.
4. **Gradient bound:**  $\|\partial \boldsymbol{\mu} / \partial \mathbf{r}\|_{\infty} \leq p_{\max}/4$ .

The proof is given in Appendix A.1. The ordering property preserves a canonical Müntz-like structure and facilitates enforcing the divergence condition via regularization, while the gradient bound prevents instabilities during optimization.

### 3.3 Müntz Divergence Regularizer

The Müntz condition  $\sum_k 1/\lambda_k = \infty$  ensures basis completeness. For finite  $K$ , we encourage configurations that would satisfy this condition asymptotically.

**Definition 6** (Müntz Divergence). *For exponents  $\boldsymbol{\mu} \in \mathbb{R}_{>0}^{K_e}$  and  $\boldsymbol{\lambda} \in \mathbb{R}_{>0}^{K_o}$ :*

$$D(\boldsymbol{\mu}, \boldsymbol{\lambda}) = \sum_{k=1}^{K_e} \frac{1}{\mu_k} + \sum_{k=1}^{K_o} \frac{1}{\lambda_k}. \quad (6)$$

**Definition 7** (Müntz Regularizer). *For threshold  $C > 0$ :*

$$\mathcal{R}_{\text{Müntz}}(\boldsymbol{\mu}, \boldsymbol{\lambda}) = \text{ReLU}(C - D(\boldsymbol{\mu}, \boldsymbol{\lambda})). \quad (7)$$

**Proposition 2** (Regularizer Effect). *The regularizer  $\mathcal{R}_{\text{Müntz}}$  encourages:*

1. **Small exponents:** To maximize  $D$ , some  $\mu_k$  should be small (near zero).

2. **Diverse exponents:** Spreading exponents increases  $D$  compared to concentration at a single value.

Both effects align with the Müntz condition's requirement for diverse, slowly-growing exponents. We set  $C = 2$  in experiments, which for  $K = 6$  exponents requires an average exponent value below 3.0, sufficient to encourage at least one small exponent near zero while allowing others to capture higher-order behavior. Preliminary experiments showed robust performance for  $C \in [1, 5]$ .

**Remark 2.** *This regularizer is not required for universal approximation but improves optimization stability and encourages diverse exponent configurations in finite networks. It serves as a soft constraint guiding the learned exponents toward configurations consistent with the classical theory.*

### 3.4 Training Objective and Stabilization

**Training Objective.** For PINNs:

$$\mathcal{L} = \mathcal{L}_{\text{PDE}} + \lambda_{\text{BC}} \mathcal{L}_{\text{BC}} + \beta_1 \mathcal{R}_{\text{Müntz}} + \beta_2 (\|\mathbf{a}\|_1 + \|\mathbf{b}\|_1), \quad (8)$$

where the  $L^1$  penalty promotes coefficient sparsity. For supervised regression, we use  $\mathcal{L}_{\text{MSE}}$  in place of  $\mathcal{L}_{\text{PDE}} + \lambda_{\text{BC}} \mathcal{L}_{\text{BC}}$ .

**Training Stabilization.** Learning exponents introduces optimization challenges. We employ three techniques:

1. **Two-time-scale optimization:** Exponents evolve slowly ( $\eta_{\text{exp}} = 0.02\eta$ ) while coefficients adapt faster ( $\eta_{\text{coeff}} = \eta$ ).
2. **Exponent warmup:** During the first  $T_{\text{warm}}$  steps, exponents are frozen to allow coefficients to find a reasonable configuration.
3. **Exponent gradient clipping:** We clip exponent gradients separately with a small threshold  $\delta \in [0.03, 0.1]$ .

Algorithm 1 summarizes the training procedure.

## 4 Theoretical Analysis

We establish universal approximation and derive approximation rates demonstrating MSN's advantages for singular functions.

### 4.1 Universal Approximation

**Theorem 3** (Universal Approximation). *Let  $f \in C([-1, 1]^d)$  and  $\varepsilon > 0$ . There exists an MSN  $f_{\text{MSN}}$  with finite depth, finite width, and exponents satisfying the Müntz condition such that  $\|f - f_{\text{MSN}}\|_{\infty} < \varepsilon$ .*

---

**Algorithm 1** MSN Training for PINNs

---

**Require:** PDE operator  $\mathcal{N}$ , BC operator  $\mathcal{B}$ , collocation points  $\{x_i^c\}$ , boundary points  $\{x_j^b\}$   
**Require:** Learning rate  $\eta$ , warmup steps  $T_{\text{warm}}$ , exponent clip  $\delta$

- 1: Initialize MSN  $f_\theta$  with random coefficients  $(\mathbf{a}, \mathbf{b})$  and exponents  $(\mathbf{r}_e, \mathbf{r}_o)$
- 2: **for**  $t = 1, \dots, T$  **do**
- 3:   Compute exponents:  $\boldsymbol{\mu} \leftarrow \text{BoundedMap}(\mathbf{r}_e)$ ,  $\boldsymbol{\lambda} \leftarrow \text{BoundedMap}(\mathbf{r}_o)$
- 4:   Compute losses:  $\mathcal{L}_{\text{PDE}}, \mathcal{L}_{\text{BC}}, \mathcal{R}_{\text{M\"untz}}$
- 5:    $\mathcal{L} \leftarrow \mathcal{L}_{\text{PDE}} + \lambda_{\text{BC}} \mathcal{L}_{\text{BC}} + \beta_1 \mathcal{R}_{\text{M\"untz}} + \beta_2 (\|\mathbf{a}\|_1 + \|\mathbf{b}\|_1)$
- 6:   Compute gradients  $\nabla_\theta \mathcal{L}$
- 7:   **if**  $t > T_{\text{warm}}$  **then**
- 8:     Clip exponent gradients:  $\nabla_{\mathbf{r}_e, \mathbf{r}_o} \mathcal{L} \leftarrow \text{ClipNorm}(\nabla_{\mathbf{r}_e, \mathbf{r}_o} \mathcal{L}, \delta)$
- 9:     Update exponents:  $\mathbf{r}_e \leftarrow \mathbf{r}_e - 0.02\eta \cdot \nabla_{\mathbf{r}_e} \mathcal{L}$ ,  $\mathbf{r}_o \leftarrow \mathbf{r}_o - 0.02\eta \cdot \nabla_{\mathbf{r}_o} \mathcal{L}$
- 10:   **end if**
- 11:   Update coefficients:  $(\mathbf{a}, \mathbf{b}, \mathbf{c}) \leftarrow (\mathbf{a}, \mathbf{b}, \mathbf{c}) - \eta \cdot \nabla_{\mathbf{a}, \mathbf{b}, \mathbf{c}} \mathcal{L}$
- 12: **end for**
- 13: **return** Trained MSN  $f_\theta$

---

*Proof Sketch.* By Theorem 2, Müntz systems (including the constant function) are dense in  $C[-1, 1]$ . Tensor products of dense univariate systems are dense in  $C([-1, 1]^d)$ . MSN layers compute sums of univariate Müntz functions with bias terms providing the constant, and the inter-layer nonlinearity  $\tau = \tanh$  provides additional expressivity. Standard UAT arguments [Cybenko, 1989, Hornik, 1991] complete the proof. Full details in Appendix A.2.  $\square$

**Remark 3** (Role of Inter-Layer Nonlinearity). *While a single MSN layer already defines a rich approximation space via Müntz polynomials, inter-layer nonlinearities ( $\tanh$ ) ensure closure under composition and simplify multivariate approximation. This design aligns MSN with standard neural network architectures while preserving the power-law expressivity of Müntz bases within each layer.*

## 4.2 Approximation Rates for Power Functions

The key advantage of MSN is not merely universal approximation (MLPs also satisfy this) but rather the *rate* of approximation for singular function classes.

**Proposition 3** (MLP Approximation Limits). *For  $f(x) = |x|^\alpha$  with  $0 < \alpha < 1$ :*

- *Networks with smooth activations ( $\tanh$ , sigmoid) require  $\Omega(N^{1/\alpha})$  neurons to achieve  $\mathcal{O}(1/N)$  error.*
- *ReLU networks with  $P$  linear pieces achieve error  $\mathcal{O}(P^{-2})$  with matching lower bound  $\Omega(P^{-2})$ .*

**Remark 4.** *The ReLU bound is stated in terms of the number of linear pieces  $P$ , not the number of neurons  $N$ . For deep ReLU networks,  $P$  can grow exponentially*

in depth while  $N$  grows linearly, so bounds written solely in terms of neurons can be misleading. The  $\mathcal{O}(P^{-2})$  rate reflects the fundamental limitation of piecewise-linear approximation.

This follows from Yarotsky [2017] and DeVore et al. [2021]. The limitation arises because smooth and piecewise-linear functions cannot efficiently represent the cusp at  $x = 0$ .

In contrast, MSN achieves dramatically better rates:

**Theorem 4** (MSN Approximation Rate). *Let  $f(x) = x^\alpha$  for  $\alpha > -1/2$ . For an MSN edge with even exponents  $\boldsymbol{\mu} = (\mu_1, \dots, \mu_K)$  where  $\mu_k > -1/2$  are distinct:*

$$\inf_{\mathbf{a} \in \mathbb{R}^K} \left\| f - \sum_{k=1}^K a_k x^{\mu_k} \right\|_{L^2[0,1]}^2 = \frac{1}{2\alpha + 1} \prod_{k=1}^K \left( \frac{\alpha - \mu_k}{\alpha + \mu_k + 1} \right)^2. \quad (9)$$

In particular:

1. If  $\mu_j = \alpha$  for some  $j$ , the error is exactly zero.
2. If  $\min_k |\mu_k - \alpha| = \delta$ , the error scales as  $\mathcal{O}(\delta^2)$ .

*Proof Sketch.* The optimal coefficients  $\mathbf{a}^*$  are the  $L^2$  projection onto  $\text{span}\{x^{\mu_1}, \dots, x^{\mu_K}\}$ . Using the Gram matrix  $G_{jk} = \langle x^{\mu_j}, x^{\mu_k} \rangle = 1/(\mu_j + \mu_k + 1)$  and projection  $b_k = \langle f, x^{\mu_k} \rangle = 1/(\alpha + \mu_k + 1)$ , the residual norm follows from standard linear algebra. For  $K = 1$ , direct computation yields error  $(\alpha - \mu)^2 / [(2\alpha + 1)(\alpha + \mu + 1)^2]$ . The product formula for general  $K$  follows from Cauchy determinant expressions; see Borwein and Erdélyi [1995] for related results on Müntz polynomial approximation. Full proof in Appendix A.3.  $\square$

**Corollary 1** (Exponential Gap). *For  $f(x) = |x|^\alpha$  with  $0 < \alpha < 1$ :*

- ReLU MLPs require  $\mathcal{O}(\varepsilon^{-1/2})$  linear pieces for error  $\varepsilon$ .
- MSN achieves error  $\varepsilon$  with  $K = 1$  exponent when  $|\mu_1 - \alpha| = \mathcal{O}(\sqrt{\varepsilon})$ .

Thus, MSN achieves with  $\mathcal{O}(1)$  parameters what requires  $\mathcal{O}(\varepsilon^{-1/2})$  piecewise-linear complexity.

**Interpretation.** Theorem 4 shows that if MSN learns an exponent close to the target power  $\alpha$ , the approximation error is quadratically small in the exponent mismatch. Since gradient descent can minimize this mismatch, MSN can discover and exploit the natural power structure of the target function. Figure 4 visualizes this error landscape, showing the zero-error diagonal where  $\mu = \alpha$  and illustrating how gradient descent navigates toward this optimal configuration.

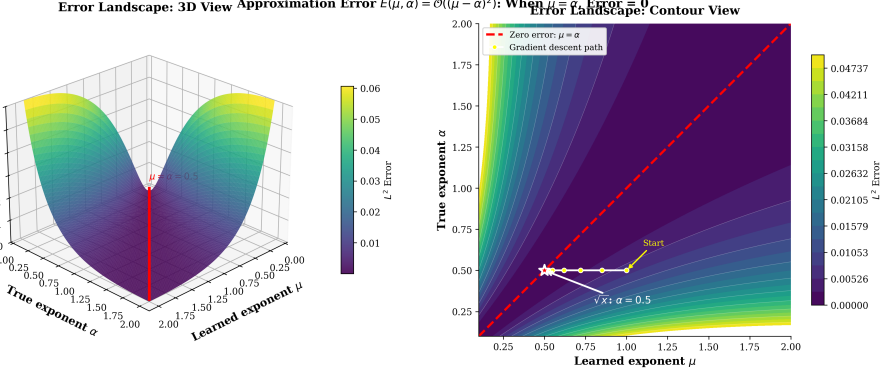


Figure 4: **Error landscape**  $E(\mu, \alpha) = \mathcal{O}((\mu - \alpha)^2)$ . (Left) 3D surface showing the  $L^2$  approximation error as a function of learned exponent  $\mu$  and true exponent  $\alpha$ . The red line marks the zero-error diagonal where  $\mu = \alpha$ . (Right) Contour view with a gradient descent trajectory showing how MSN learns  $\mu \rightarrow \alpha$ . When the learned exponent matches the true exponent, the error is exactly zero. This is the key insight enabling MSN’s dramatic efficiency gains over MLPs.

## 5 Experiments

We evaluate MSN on supervised regression and PINN benchmarks, focusing on problems where singular or fractional behavior is expected. All experiments use 3 random seeds; we report mean  $\pm$  std. Code is available at <https://github.com/ReFractals/muntz-szasz-networks>.

### 5.1 Experimental Setup

**Baselines.** We compare against:

- **MLP (big):** Standard MLP with hidden dimension 64, depth 3 (4,353 parameters).
- **MLP (param-matched):** MLP with hidden dimension chosen to match MSN’s parameter count.

**MSN Configuration.** Unless otherwise specified:  $K_e = K_o = 6$  exponents, bounded mode with  $p_{\max} = 2.0$  to 4.0, layer-wise exponent sharing. For PINNs: warmup 500-1500 steps, exponent learning rate  $0.02\eta$  to  $0.1\eta$ , gradient clip  $\delta = 0.03$  to 0.1.

### 5.2 Supervised Regression

We consider three target functions of increasing difficulty:

- $f_1(x) = \sqrt{x}$  : singular derivative at  $x = 0$

Table 1: **Supervised regression results.** RMSE (mean  $\pm$  std over 3 seeds). MSN achieves 5-8 $\times$  lower error on singular functions while remaining competitive on smooth functions. Param-matched comparisons confirm the advantage is architectural, not from capacity.

Task	Model	RMSE	Params
$\sqrt{x}$	MSN	<b>0.00224 <math>\pm</math> 0.0005</b>	425
	MSN (no Müntz)	0.00399 $\pm$ 0.0038	425
	MSN (cumsum)	0.00498 $\pm$ 0.0039	425
	MLP (big)	0.01043 $\pm$ 0.0028	4,353
	MLP (param-matched)	0.01788 $\pm$ 0.0004	438
cusp	MSN	<b>0.00500 <math>\pm</math> 0.0007</b>	1,489
	MSN (no Müntz)	0.00427 $\pm$ 0.0005	1,489
	MSN (cumsum)	0.00630 $\pm$ 0.0039	1,489
	MLP (big)	0.02175 $\pm$ 0.0046	4,545
	MLP (param-matched)	0.02741 $\pm$ 0.0022	1,549
sparse poly	MSN	0.00355 $\pm$ 0.0021	425
	MSN (no Müntz)	0.00727 $\pm$ 0.0003	425
	MSN (cumsum)	0.00576 $\pm$ 0.0021	425
	<b>MLP (big)</b>	<b>0.00206 <math>\pm</math> 0.0003</b>	4,353
	MLP (param-matched)	0.00728 $\pm$ 0.0021	438

- $f_2(x) = |x - 0.5|^{0.2}$  : cusp singularity at  $x = 0.5$
- $f_3(x) = x^3 + 0.5x^7$  : smooth polynomial (control)

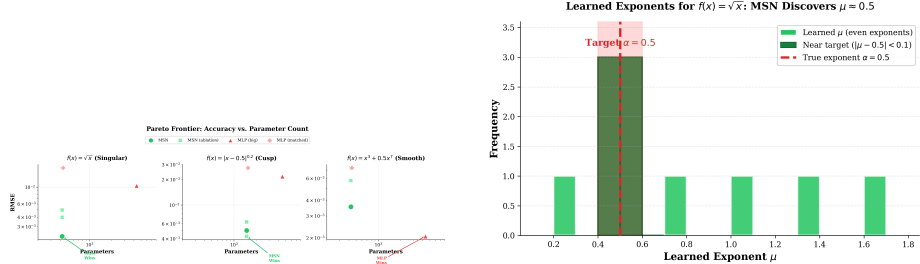
**Results.** Table 1 shows MSN achieves **4.6 $\times$**  lower error than MLP (big) and **8 $\times$**  lower than the parameter-matched MLP on  $\sqrt{x}$ . For the cusp function, improvements are **4.4 $\times$**  and **5.5 $\times$**  respectively.

Importantly, on the smooth polynomial, MLP (big) achieves the best performance. This confirms MSN’s advantage is specific to singular structure; it does not uniformly dominate but excels where its inductive bias matches the problem.

**Ablations.** Table 1 includes ablations:

- **MSN (no Müntz):** Removing the Müntz regularizer degrades performance on  $\sqrt{x}$  by 1.8 $\times$ , confirming the regularizer’s value.
- **MSN (cumsum):** The cumsum parameterization is slightly less accurate but more stable, useful for difficult optimization.

**Interpretability.** Figure 5b shows the learned exponent distribution for  $\sqrt{x}$ : exponents concentrate near  $\mu = 0.5$ , exactly matching the true power. This



(a) Pareto frontier: error vs. parameters across three tasks. MSN dominates for singular functions ( $\sqrt{x}$ , cusp) while MLP wins on smooth polynomials.

(b) Learned exponents for  $\sqrt{x}$ . The distribution concentrates near  $\mu = 0.5$ , the true exponent, demonstrating MSN’s interpretability.

Figure 5: **Supervised regression analysis.** (a) MSN achieves the best accuracy-efficiency trade-off for singular functions, with clear task separation showing when each architecture excels. (b) Learned exponents are interpretable and match the target function structure.

Table 2: **PINN results: singular ODE.** MSN achieves  $3.2\times$  lower error than MLP (big) and  $5.6\times$  lower than param-matched MLP, with  $5\times$  fewer parameters.

Model	RMSE (mean $\pm$ std)	Params
MSN	<b><math>0.0529 \pm 0.036</math></b>	825
MLP (big)	$0.1677 \pm 0.047$	4,353
MLP (param-matched)	$0.2960 \pm 0.176$	838

interpretability is a unique advantage; the network reveals the underlying solution structure.

### 5.3 PINN Benchmark: Singular ODE

We consider the singular ODE:

$$u'(x) = \frac{1}{2\sqrt{x}}, \quad u(0) = 0, \quad x \in [0, 1]. \quad (10)$$

The exact solution is  $u(x) = \sqrt{x}$ , with a singular derivative at  $x = 0$ .

**Results.** Table 2 shows MSN achieves  **$3.2\times$**  lower RMSE than MLP (big) with  **$5.3\times$**  fewer parameters. Figure 6 visualizes the solution, error profile, and learned exponents. Notably, MSN’s advantage is most pronounced near  $x = 0$ , exactly where the singularity occurs.

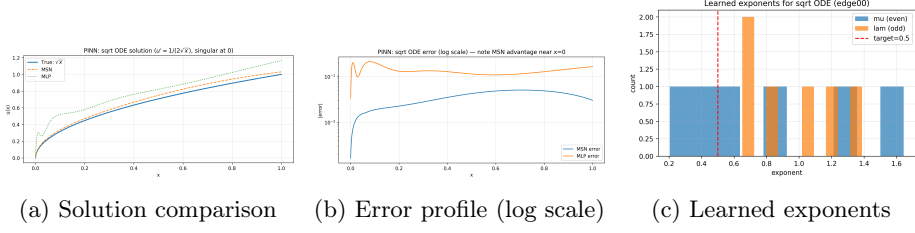


Figure 6: **PINN: singular ODE**  $u' = 1/(2\sqrt{x})$ . (a) MSN closely matches the true  $\sqrt{x}$  solution. (b) Error is lowest near  $x = 0$  where the singularity occurs. (c) Learned exponents cluster near 0.5, directly reflecting the solution structure.

Table 3: **PINN results: boundary-layer BVP.** MSN consistently outperforms MLPs across stiffness levels. At  $\epsilon = 0.01$ , all methods exhibit optimization instability, consistent with prior PINN literature.

$\epsilon$	Model	RMSE (mean $\pm$ std)	Params
0.05	MSN	<b><math>0.222 \pm 0.076</math></b>	825
	MLP (big)	$0.270 \pm 0.080$	4,353
	MLP (param-matched)	$0.334 \pm 0.110$	838
0.02	MSN	<b><math>0.416 \pm 0.049</math></b>	825
	MLP (big)	$0.472 \pm 0.005$	4,353
	MLP (param-matched)	$0.473 \pm 0.005$	838

#### 5.4 PINN Benchmark: Boundary-Layer BVP

We consider the stiff convection-diffusion problem:

$$-\epsilon u''(x) + u'(x) = 0, \quad u(0) = 0, \quad u(1) = 1, \quad x \in [0, 1], \quad (11)$$

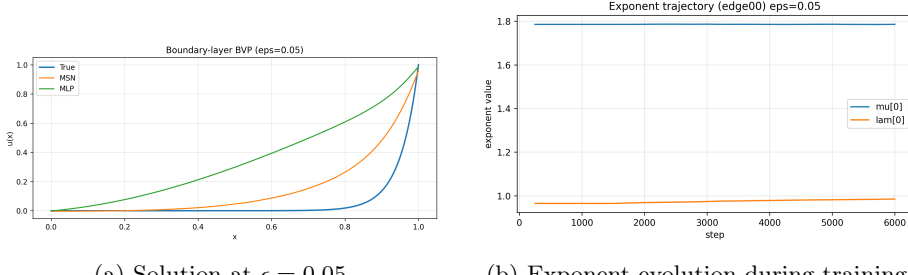
with exact solution  $u(x) = (e^{x/\epsilon} - 1)/(e^{1/\epsilon} - 1)$ . For small  $\epsilon$ , this exhibits a sharp boundary layer near  $x = 1$ .

**Results.** Table 3 shows MSN achieves **18%** lower error at  $\epsilon = 0.05$  and **12%** at  $\epsilon = 0.02$ . For  $\epsilon = 0.01$ , all methods exhibit numerical instabilities (NaN values), consistent with prior work on PINNs for stiff problems [Krishnapriyan et al., 2021, Arzani et al., 2023].

Figure 7b shows exponent trajectories during training: exponents initially explore before converging to stable values that capture the boundary layer structure.

#### 5.5 Summary of Experimental Findings

1. **Parameter efficiency:** MSN achieves  $3\text{-}8\times$  lower error with  $5\text{-}10\times$  fewer parameters on singular functions.

(a) Solution at  $\epsilon = 0.05$ 

(b) Exponent evolution during training

Figure 7: **PINN: boundary-layer BVP.** (a) MSN captures the sharp boundary layer more accurately than MLP. (b) Exponents adapt during training, initially exploring the space before converging to stable values.

2. **Interpretability:** Learned exponents match known solution structure (e.g.,  $\mu \approx 0.5$  for  $\sqrt{x}$ ).
3. **Specificity:** Advantages are specific to non-smooth functions; MLP remains competitive on smooth targets.
4. **Stabilization:** Two-time-scale optimization and warmup are crucial for reliable training.

## 6 Related Work

**Neural Network Approximation Theory.** Classical results [Cybenko, 1989, Hornik, 1991, Barron, 1993] establish universal approximation for single-hidden-layer networks. Yarotsky [2017] provides sharp rates for ReLU networks, showing  $\mathcal{O}(N^{-2s/d})$  for  $W^{s,\infty}$  functions. DeVore et al. [2021] establishes that optimal rates come at the cost of discontinuous parameter selection. Our work extends this theory to learnable power bases with explicit rates for singular functions.

**Physics-Informed Neural Networks.** PINNs [Raissi et al., 2019] solve PDEs by embedding physical constraints. Challenges include spectral bias [Wang et al., 2021b], gradient imbalance [Wang et al., 2021a], and failure on stiff problems [Krishnapriyan et al., 2021]. Solutions include Fourier features [Tancik et al., 2020], adaptive weighting [Wang et al., 2021a], and domain decomposition [Jagtap et al., 2020]. Our approach is complementary: rather than modifying training, we modify the architecture to better represent singular solutions.

**Fractional and Singular PDE Methods.** Fractional PINNs [Pang et al., 2019] handle fractional derivatives via specialized discretization. For fracture mechanics, extended PINNs [Zhu et al., 2025] embed crack-tip singularities explicitly. These methods require problem-specific knowledge; MSN learns appropriate representations from data.

**Learnable Activation Functions.** Parametric ReLU [He et al., 2015] learns a single slope parameter. SIREN [Sitzmann et al., 2020] uses periodic activations for implicit representations. Kolmogorov-Arnold Networks (KAN) [Liu et al., 2024] learn univariate functions via B-splines. MSN differs fundamentally: rather than learning *coefficients* of fixed bases (splines), we learn the *exponents* of power functions, motivated by approximation theory for singular functions.

**Müntz Polynomials in Numerical Methods.** Müntz-Galerkin methods [Shen and Wang, 2016] achieve spectral convergence for singular boundary problems. Müntz-Legendre polynomials [Borwein et al., 1994, Milovanović, 1999] provide orthogonal bases. Our work brings these classical tools into the neural network framework with end-to-end exponent learning.

## 7 Discussion

**When to Use MSN.** MSN is not intended to replace generic architectures, but to complement them when power-law structure is present or suspected. It is designed for problems where the solution exhibits singular or fractional power behavior. This includes:

- Boundary layer problems (fluid dynamics)
- Fracture and crack propagation (solid mechanics)
- Corner singularities in elliptic PDEs
- Anomalous diffusion (fractional PDEs)

For smooth problems without singular structure, standard MLPs remain competitive or superior (Table 1, sparse polynomial).

**Limitations.** Several limitations warrant discussion:

- **Very stiff problems:** At  $\epsilon = 0.01$  in the boundary-layer benchmark, all methods failed. This is a known limitation of vanilla PINNs; curriculum learning or specialized architectures may help.
- **Higher dimensions:** Current experiments are 1D. Extension to higher dimensions via tensor products or radial bases is ongoing work.
- **Computational cost:** Computing  $|x|^\mu$  for non-integer  $\mu$  requires exp-log evaluation, adding overhead compared to ReLU. However, the dramatic reduction in required neurons often compensates.

**Interpretability.** A unique advantage of MSN is that learned exponents directly reveal solution structure. In the  $\sqrt{x}$  experiments, exponents clustered near 0.5; no post-hoc interpretation required. This could enable scientific discovery in problems where the solution form is unknown.

## 8 Conclusion

We introduced Müntz-Szász Networks (MSN), a neural architecture that learns fractional power exponents grounded in classical approximation theory. MSN achieves  $3\text{-}8\times$  lower error on functions with singular behavior while using  $5\text{-}10\times$  fewer parameters than standard MLPs. The learned exponents are interpretable, directly reflecting the underlying solution structure.

Our theoretical analysis establishes universal approximation and novel approximation rates showing MSN’s fundamental advantages for power-law functions. Experiments on supervised regression and PINN benchmarks validate these advantages empirically.

MSN demonstrates that theory-guided architectural design can yield dramatic improvements for scientifically-motivated function classes. Future work includes extension to higher dimensions, application to fractional PDEs, and integration with other PINN improvements for stiff problems.

## Acknowledgments

The author thanks Bum Jun Kim (University of Tokyo) for carefully reading an earlier version of this manuscript and identifying several technical corrections, including the need to include the constant function in the Full Müntz Theorem statement, correcting the  $L^2$  projection error formula, and clarifying the MLP approximation bounds in terms of linear pieces rather than neurons. These corrections significantly improved the mathematical rigor of this work.

## References

T. L. Anderson. *Fracture Mechanics: Fundamentals and Applications*. CRC Press, 3rd edition, 2005.

Amirhossein Arzani, Kevin W. Cassel, and Roshan M. D’Souza. Theory-guided physics-informed neural networks for boundary layer problems with singular perturbation. *Journal of Computational Physics*, 473:111768, 2023.

Andrew R. Barron. Universal approximation bounds for superpositions of a sigmoidal function. *IEEE Transactions on Information Theory*, 39(3):930–945, 1993.

Peter Borwein and Tamás Erdélyi. *Polynomials and Polynomial Inequalities*, volume 161 of *Graduate Texts in Mathematics*. Springer-Verlag, New York, 1995. ISBN 978-0-387-94509-5.

Peter Borwein, Tamás Erdélyi, and John Zhang. Müntz systems and orthogonal Müntz-Legendre polynomials. *Transactions of the American Mathematical Society*, 342:523–542, 1994.

George Cybenko. Approximation by superpositions of a sigmoidal function. *Mathematics of Control, Signals, and Systems*, 2(4):303–314, 1989.

Ronald DeVore, Boris Hanin, and Guergana Petrova. Neural network approximation. *Acta Numerica*, 30:327–444, 2021.

Pierre Grisvard. *Elliptic Problems in Nonsmooth Domains*. Classics in Applied Mathematics. SIAM, 2011.

Kaiming He, Xiangyu Zhang, Shaoqing Ren, and Jian Sun. Delving deep into rectifiers: Surpassing human-level performance on ImageNet classification. In *IEEE International Conference on Computer Vision (ICCV)*, pages 1026–1034, 2015.

Kurt Hornik. Approximation capabilities of multilayer feedforward networks. *Neural Networks*, 4(2):251–257, 1991.

Ameya D. Jagtap, Ehsan Kharazmi, and George E. Karniadakis. Conservative physics-informed neural networks on discrete domains for conservation laws: Applications to forward and inverse problems. *Computer Methods in Applied Mechanics and Engineering*, 365:113028, 2020.

Aditi S. Krishnapriyan, Amir Gholami, Shandian Zhe, Robert M. Kirby, and Michael W. Mahoney. Characterizing possible failure modes in physics-informed neural networks. In *Advances in Neural Information Processing Systems (NeurIPS)*, volume 34, pages 26548–26560, 2021.

Ziming Liu, Yixuan Wang, Sachin Vaidya, Fabian Ruehle, James Halverson, Marin Soljačić, Thomas Y. Hou, and Max Tegmark. KAN: Kolmogorov-Arnold networks. *arXiv preprint arXiv:2404.19756*, 2024.

George G. Lorentz, Manfred von Golitschek, and Yuly Makovoz. *Constructive Approximation: Advanced Problems*, volume 304 of *Grundlehren der mathematischen Wissenschaften*. Springer-Verlag, Berlin, 1996.

Gradimir V. Milovanović. Müntz orthogonal polynomials and their numerical evaluation. In W. Gautschi, G. Opfer, and G. H. Golub, editors, *Applications and Computation of Orthogonal Polynomials*, volume 131 of *ISNM*, pages 179–194. Birkhäuser, Basel, 1999.

Ch. H. Müntz. Über den Approximationssatz von Weierstrass. In *H. A. Schwarz's Festschrift*, pages 303–312. Berlin, 1914.

Guofei Pang, Lu Lu, and George E. Karniadakis. fPINNs: Fractional physics-informed neural networks. *SIAM Journal on Scientific Computing*, 41(4):A2603–A2626, 2019.

Nasim Rahaman, Aristide Baratin, Devansh Arpit, Felix Draxler, Min Lin, Fred Hamprecht, Yoshua Bengio, and Aaron Courville. On the spectral bias of neural networks. In *International Conference on Machine Learning (ICML)*, volume 97 of *PMLR*, pages 5301–5310, 2019.

Maziar Raissi, Paris Perdikaris, and George E. Karniadakis. Physics-informed neural networks: A deep learning framework for solving forward and inverse problems involving nonlinear partial differential equations. *Journal of Computational Physics*, 378:686–707, 2019.

Hermann Schlichting and Klaus Gersten. *Boundary-Layer Theory*. Springer, 9th edition, 2017.

Jie Shen and Yingwei Wang. Müntz-Galerkin methods and applications to mixed Dirichlet-Neumann boundary value problems. *SIAM Journal on Scientific Computing*, 38(4):A2357–A2381, 2016.

Vincent Sitzmann, Julien N. P. Martel, Alexander W. Bergman, David B. Lindell, and Gordon Wetzstein. Implicit neural representations with periodic activation functions. In *Advances in Neural Information Processing Systems (NeurIPS)*, volume 33, pages 7462–7473, 2020.

Otto Szász. Über die Approximation stetiger Funktionen durch lineare Aggregate von Potenzen. *Mathematische Annalen*, 77(4):482–496, 1916.

Matthew Tancik, Pratul P. Srinivasan, Ben Mildenhall, Sara Fridovich-Keil, Nithin Raghavan, Utkarsh Singhal, Ravi Ramamoorthi, Jonathan T. Barron, and Ren Ng. Fourier features let networks learn high frequency functions in low dimensional domains. In *Advances in Neural Information Processing Systems (NeurIPS)*, volume 33, pages 7537–7547, 2020.

Sifan Wang, Yujun Teng, and Paris Perdikaris. Understanding and mitigating gradient flow pathologies in physics-informed neural networks. *SIAM Journal on Scientific Computing*, 43(5):A3055–A3081, 2021a.

Sifan Wang, Hanwen Wang, and Paris Perdikaris. On the eigenvector bias of Fourier feature networks: From regression to solving multi-scale PDEs with physics-informed neural networks. *Computer Methods in Applied Mechanics and Engineering*, 384:113938, 2021b.

Dmitry Yarotsky. Error bounds for approximations with deep ReLU networks. *Neural Networks*, 94:103–114, 2017.

Bokai Zhu, Hengguang Li, and Qinghui Zhang. Extended physics-informed extreme learning machine for linear elastic fracture mechanics. *Computer Methods in Applied Mechanics and Engineering*, 435:117655, 2025.

## A Proofs

### A.1 Proof of Proposition 1 (Bounded Parameterization)

*Proof.* (1) **Strict positivity.** For any  $r \in \mathbb{R}$ ,  $\sigma(r) = 1/(1 + e^{-r}) \in (0, 1)$ . The sorted values also lie in  $(0, 1)$ , so

$$\mu_k = \varepsilon + (p_{\max} - 2\varepsilon) \cdot s_k \in (\varepsilon, p_{\max} - \varepsilon).$$

(2) **Ordering.** The sorting operation ensures  $s_1 \leq s_2 \leq \dots \leq s_K$ . For inputs drawn from continuous distributions (or with probability 1 under gradient noise), sigmoid outputs are distinct, giving strict inequality.

(3) **Differentiability.** The sigmoid  $\sigma$  is smooth. Sorting is piecewise linear, differentiable except when two sigmoid outputs coincide (a measure-zero set).

(4) **Gradient bound.** We have  $\sigma'(r) = \sigma(r)(1 - \sigma(r)) \leq 1/4$  (maximum at  $r = 0$ ). The sorting Jacobian has entries in  $\{0, 1\}$ , so

$$\left| \frac{\partial \mu_k}{\partial r_j} \right| = (p_{\max} - 2\varepsilon) \cdot \left| \frac{\partial s_{\pi(k)}}{\partial r_j} \right| \leq (p_{\max} - 2\varepsilon) \cdot \frac{1}{4} < \frac{p_{\max}}{4}. \quad \square$$

### A.2 Proof of Theorem 3 (Universal Approximation)

*Proof.* Step 1: **Univariate density.** By Theorem 2, the system  $\{1\} \cup \{|x|^{\mu_k}\} \cup \{\text{sign}(x)|x|^{\lambda_k}\}$  with  $\sum_k 1/\mu_k + \sum_k 1/\lambda_k = \infty$  is dense in  $C[-1, 1]$ . The constant function 1 is essential for approximating functions with  $f(0) \neq 0$ .

Step 2: **Multivariate extension.** Consider  $f \in C([-1, 1]^d)$ . By Stone-Weierstrass, finite sums of products  $\prod_{i=1}^d g_i(x_i)$  with  $g_i \in C[-1, 1]$  are dense in  $C([-1, 1]^d)$ .

Each  $g_i$  can be approximated by a Müntz combination:

$$g_i(x_i) \approx c_{i0} + \sum_{k=1}^{K_i} a_{ik} |x_i|^{\mu_k} + \sum_{k=1}^{K_i} b_{ik} \text{sign}(x_i) |x_i|^{\lambda_k}.$$

**Step 3: Network realization.** An MSN layer computes sums of univariate Müntz functions, and the bias terms  $c_j$  in Definition 3 provide the constant functions needed for completeness. The inter-layer nonlinearity  $\tau = \tanh$  is non-polynomial, so by standard UAT arguments [Cybenko, 1989, Hornik, 1991], compositions of MSN layers can approximate any continuous function on compact domains.  $\square$

### A.3 Proof of Theorem 4 (Approximation Rate)

*Proof.* We compute the  $L^2[0, 1]$  projection of  $f(x) = x^\alpha$  onto  $\text{span}\{x^{\mu_1}, \dots, x^{\mu_K}\}$ .

**Step 1: Gram matrix.** The Gram matrix has entries:

$$G_{jk} = \langle x^{\mu_j}, x^{\mu_k} \rangle_{L^2} = \int_0^1 x^{\mu_j + \mu_k} dx = \frac{1}{\mu_j + \mu_k + 1}.$$

**Step 2: Projection coefficients.** The right-hand side vector is:

$$b_k = \langle f, x^{\mu_k} \rangle = \int_0^1 x^{\alpha+\mu_k} dx = \frac{1}{\alpha + \mu_k + 1}.$$

Optimal coefficients satisfy  $G\mathbf{a}^* = \mathbf{b}$ .

**Step 3: Residual norm.** The squared projection error is:

$$\|f - \hat{f}\|_{L^2}^2 = \|f\|_{L^2}^2 - \mathbf{b}^\top G^{-1} \mathbf{b} = \frac{1}{2\alpha + 1} - \mathbf{b}^\top G^{-1} \mathbf{b}.$$

**Step 4: Explicit formula for  $K = 1$ .** With single exponent  $\mu$ , we have  $G = 1/(2\mu + 1)$  and  $b = 1/(\alpha + \mu + 1)$ , so

$$a^* = b/G = \frac{2\mu + 1}{\alpha + \mu + 1}.$$

The squared error is:

$$\begin{aligned} \|f - a^* x^\mu\|_{L^2}^2 &= \|f\|_{L^2}^2 - \frac{b^2}{G} = \frac{1}{2\alpha + 1} - \frac{(2\mu + 1)}{(\alpha + \mu + 1)^2} \\ &= \frac{(\alpha + \mu + 1)^2 - (2\mu + 1)(2\alpha + 1)}{(2\alpha + 1)(\alpha + \mu + 1)^2} \\ &= \frac{(\alpha - \mu)^2}{(2\alpha + 1)(\alpha + \mu + 1)^2}. \end{aligned}$$

If  $\mu = \alpha$ , the numerator vanishes: error is exactly zero. If  $\mu = \alpha + \delta$  for small  $\delta$ , the error is  $\mathcal{O}(\delta^2)$ .

**Step 5: General  $K$ .** For multiple exponents, the product formula (9) follows from the determinant expression for projection residuals. The squared distance to  $\text{span}\{x^{\mu_1}, \dots, x^{\mu_K}\}$  can be written as a ratio of Gram determinants. Using the Cauchy determinant formula for matrices of the form  $G_{jk} = 1/(\mu_j + \mu_k + 1)$ , one obtains the stated product expression; see Borwein and Erdélyi [1995] for background on Müntz polynomial approximation theory.  $\square$

#### A.4 Proof of Proposition 2 (Regularizer Effect)

*Proof.* (1) **Small exponents.** The divergence  $D = \sum_k 1/\mu_k$  increases when  $\mu_k$  decreases. To satisfy  $D \geq C$  (making  $\mathcal{R} = 0$ ), the optimizer pushes some exponents toward small values.

(2) **Diversity.** For  $K$  exponents all equal to  $\mu^*$ :  $D = K/\mu^*$ . For diverse exponents  $\{\mu_1, \dots, \mu_K\}$  with  $\mu_1 < \mu^* < \mu_K$ :

$$D = \sum_k \frac{1}{\mu_k} > \frac{K}{\mu^*}$$

by convexity of  $1/\mu$ . Thus diversity increases  $D$ , helping satisfy the constraint.  $\square$

## B Additional Experimental Details

### B.1 Hyperparameter Settings

Table 4: Hyperparameters for all experiments.

Parameter	Supervised	PINN
Learning rate $\eta$	$2 \times 10^{-3}$	$2 \times 10^{-3}$
Exponent LR multiplier	1.0	0.02-0.1
Training steps	2,000	3,000-6,000
Warmup steps	0	500-1,500
Exponent gradient clip $\delta$	-	0.03-0.1
$K_e$ (even exponents)	6	6
$K_o$ (odd exponents)	6	6
$p_{\max}$	2.0-8.0	2.0-3.0
$\beta_1$ (Müntz reg.)	$10^{-2}$	$10^{-2}$
$\beta_2$ ( $L^1$ reg.)	$10^{-4}$	$10^{-4}$
$\lambda_{\text{BC}}$	-	200 (adaptive)
Collocation points	-	2,048
Boundary points	-	256

### B.2 Computational Resources

All experiments were conducted on a single NVIDIA A100 GPU. Supervised regression and singular ODE experiments complete in approximately 60-90 minutes total. The boundary-layer BVP experiments require 9-10 hours due to the increased training steps and multiple stiffness values. MSN training is slightly slower per iteration than MLP due to exp-log evaluation of  $|x|^\mu$ , but requires far fewer parameters for comparable accuracy.

### B.3 Additional Experimental Results

This section provides supplementary visualizations for the experiments presented in the main text.

### B.3.1 Supervised Regression

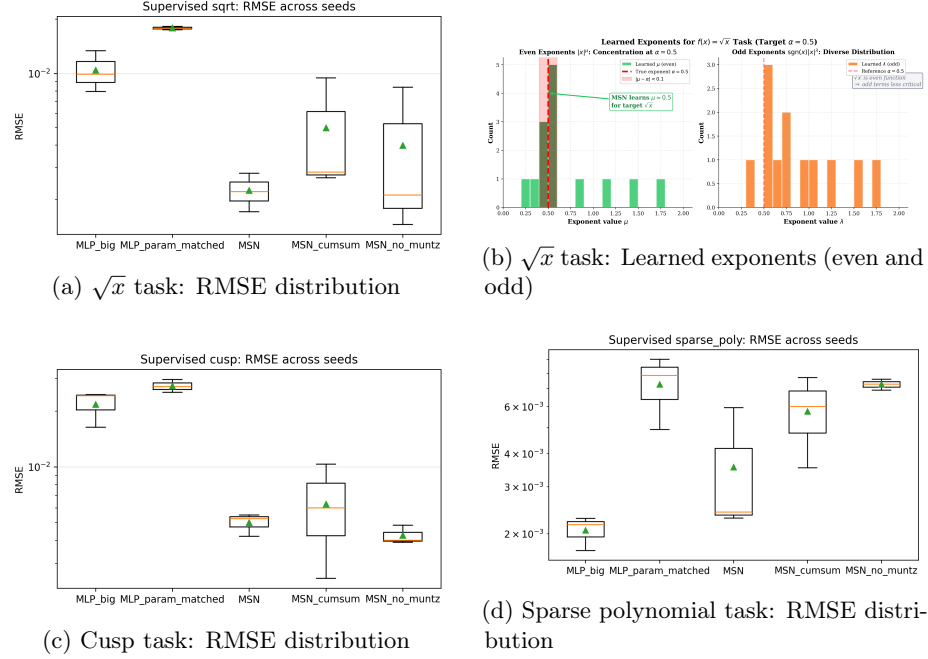


Figure 8: **Supervised regression: detailed results.** (a,c,d) RMSE distributions across 3 random seeds for each task, showing MSN’s consistent advantage on singular functions ( $\sqrt{x}$ , cusp) and comparable performance on smooth functions (sparse polynomial). (b) Histogram of learned exponents for  $\sqrt{x}$ , showing concentration of even exponents near the true exponent  $\mu = 0.5$ , while odd exponents remain diverse (as expected for the even function  $\sqrt{x}$ ).

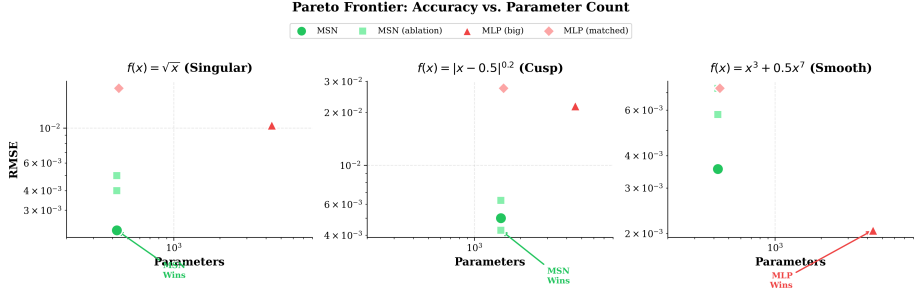


Figure 9: **Pareto frontier: accuracy vs. parameter count.** MSN achieves the best trade-off for singular functions ( $\sqrt{x}$ , cusp), reaching lower error with fewer parameters than both MLP variants. For the smooth polynomial task, MLP (big) achieves the best performance, confirming that MSN’s advantage is specific to singular structure. Each subplot shows a different task with clear winner annotations.

### B.3.2 PINN: Singular ODE

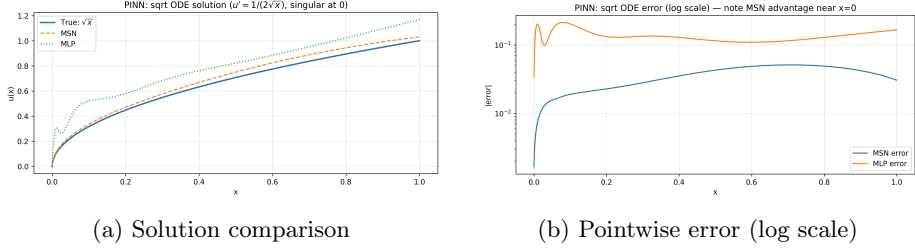


Figure 10: **Singular ODE  $u' = 1/(2\sqrt{x})$ : solution quality.** (a) MSN closely tracks the true  $\sqrt{x}$  solution, while MLP exhibits visible deviation. (b) Pointwise error on log scale shows MSN achieves lower error across the domain, particularly near the singularity at  $x = 0$ .

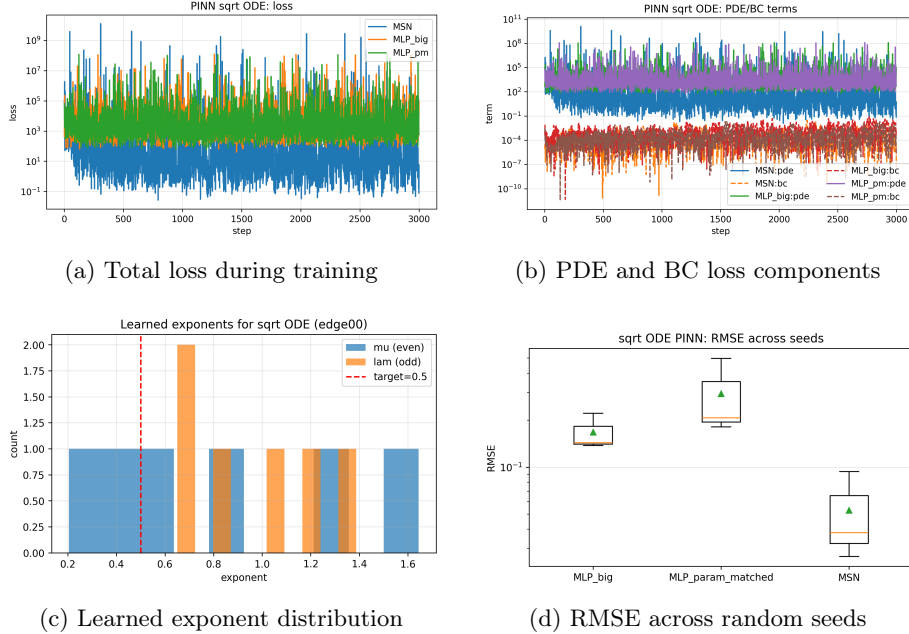


Figure 11: **Singular ODE: training dynamics.** (a) MSN converges to lower total loss than MLP. (b) Both PDE residual and boundary condition losses decrease faster for MSN. (c) Learned exponents concentrate near  $\mu \approx 0.5$ , matching the true solution structure. (d) RMSE distribution across 3 seeds confirms consistent MSN advantage.

### B.3.3 PINN: Boundary-Layer BVP

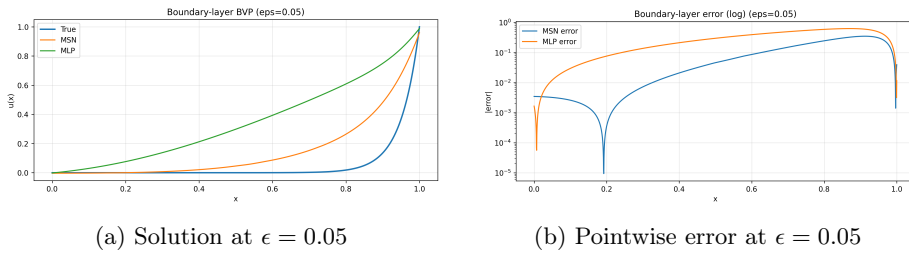
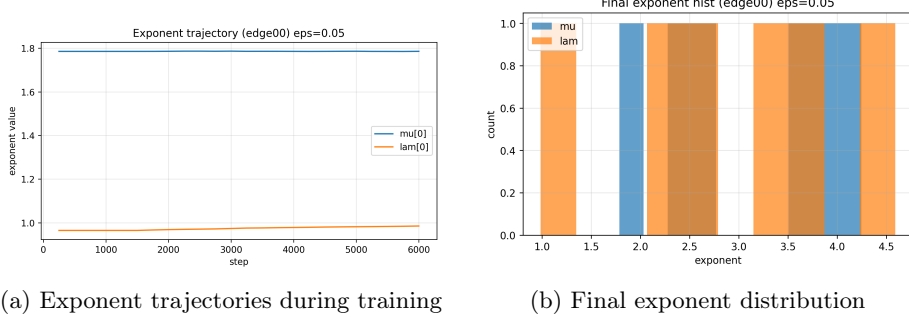


Figure 12: **Boundary-layer BVP: solution quality.** (a) MSN captures the sharp boundary layer near  $x = 1$  more accurately than MLP. (b) Error is concentrated in the boundary layer region for both methods, but MSN achieves lower peak error.



(a) Exponent trajectories during training (b) Final exponent distribution

Figure 13: **Boundary-layer BVP: exponent dynamics.** (a) Exponents evolve during training, initially exploring before converging to stable values. The warmup period (first 500 steps) freezes exponents to allow coefficient adaptation. (b) Final exponent distribution shows diversity, with some exponents adapting to capture the boundary layer structure.

#### B.3.4 Gradient Diagnostics

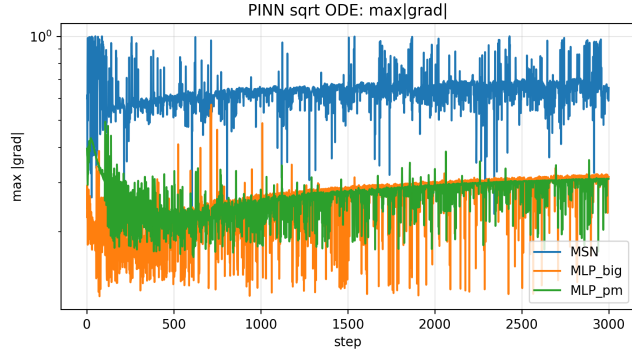


Figure 14: **Gradient diagnostics for singular ODE.** Gradient norms for coefficient parameters and exponent parameters during training. The two-time-scale optimization (exponent learning rate = 0.02× coefficient learning rate) and gradient clipping maintain stable training despite the challenging singular structure.